Enhanced electrocatalytic production of H_2O_2 at Co-based air-diffusion cathodes for the photoelectro-Fenton treatment of bronopol

Zhihong Ye [1], Diego R. V. Guelfi [1], Garbiñe Álvarez [2], Francisco Alcaide [2], Enric Brillas [1], Ignasi Sirés [1,*]

[1] *Laboratori d'Electroquímica dels Materials i del Medi Ambient, Departament de Química Física, Facultat de Química, Universitat de Barcelona, Martí i Franquès 1-11, 08028 Barcelona, Spain*

[2] *CIDETEC, Paseo Miramón 196, 20014 San Sebastián, Spain*

Paper submitted to be published in *Applied Catalysis B: Environmental*

*Corresponding author: Tel.: +34 934039240; fax: +34 934021231.

E-mail address: i.sires@ub.edu (I. Sirés)

Abstract

(Co, S, P)-decorated multiwalled carbon nanotubes (MWCNTs) have been synthesized following a hydrothermal route as electrocatalysts to manufacture large surface area air-diffusion cathodes with carbon cloth as substrate. The enhanced electrocatalytic H_2O_2 production as compared with Co-free MWCNTs cathodes was demonstrated in a 2.5-L pre-pilot plant with either a RuO_2-based or boron-doped diamond (BDD) anode, accumulating between 2- and 3-fold greater H_2O_2 contents with the catalyzed cathode. The good stability of this new material was ensured from the low Co leaching, with less than 9% Co released to solutions upon repeated usage. Aqueous solutions of the brominated organic preservative bronopol with 0.050 M Na_2SO_4 at pH 3.0 were comparatively treated by electro-oxidation (EO-H_2O_2), electro-Fenton (EF), UVA-assisted photoelectro-Fenton (PEF) and solar PEF (SPEF) at constant current density. SPEF with BDD anode and the catalyzed cathode showed the best performance, with total bronopol removal at 210 min and 94% mineralization after 360 min at 40 mA cm^{-2}, thanks to the action of $^{\bullet}OH$, BDD($^{\bullet}OH$) and sunlight. Formic acid was identified as main reaction by-product, whereas Br and N atoms were mainly converted to Br^-, BrO_3^- and NO_3^-. Some unidentified organic by-product containing Br and N was formed as well.

1. Introduction

H_2O_2 is one of the most versatile commodities with worldwide use in many end-use industries, including pulp and paper, custom synthesis and fine chemicals, textile, environmental, and others [1]. According to recent H_2O_2 market surveys, growth opportunities are clearly envisaged in the near future [2]. Within this framework, the electrochemical H_2O_2 production has emerged as an alternative to the classical anthraquinone method, since it prevents the use of toxic organic solvents needed in that synthesis as well as stabilizers that minimize its decomposition but are usually undesirable for many applications. Moreover, the explosion risks from storage and transportation of highly concentrated H_2O_2 solutions are reduced [3]. Off-site H_2O_2 electrogeneration finds an important application in advanced oxidation processes (AOPs) such as H_2O_2/UVC, H_2O_2/Fe^{2+} (UVA) and H_2O_2/O_3 for the removal of organic contaminants from wastewater [4,5]. Nonetheless, much progress has been made in recent years on the on-site environmental applications. In particular, the so-called Fenton-based electrochemical AOPs (EAOPs) like electro-Fenton (EF) and UVA or solar photoelectro-Fenton (PEF or SPEF), are extremely effective to produce a powerful and clean oxidant like $^\bullet$OH from Fenton's reaction (1) upon continuous and controlled H_2O_2 generation [6-8].

$$Fe^{2+} + H_2O_2 \rightarrow Fe^{3+} + {}^\bullet OH + OH^- \tag{1}$$

Traditionally, cheap carbonaceous materials like graphite [9], carbon felt [10-12] and reticulated vitreous carbon [11,13] have shown ability to produce H_2O_2 from the two-electron reduction of dissolved O_2 via reaction (2). However, much higher efficiency has been demonstrated upon atmospheric air supply: (i) through an air chamber that feeds a hydrophobized air-diffusion cathode [14-19] and (ii) to super-saturate the solutions with O_2 by means of a jet aerator [20] or high-pressure devices [21]. Some of these setups allow the fast

56   accumulation of H_2O_2 with more than 90% current efficiency [18]. Significant advances have

57   been achieved by the design of more efficient H_2O_2 electrolyzers [3] and the introduction of

58   nanocarbons, either pristine or chemically modified, like carbon fibers [22], carbon nanotubes

59   [23,24] or graphene [25-27], among others, because the increased electroactive surface area of

60   the cathode enhances the O_2 mass transport rate.

61    $O_{2(g)} + 2H^+ + 2e^- \rightarrow H_2O_2$ (2)

62   The EF treatment of organic pollutants employing an air-diffusion cathode has usually been

63   carried out with pristine carbon, at either small [28] or pre-pilot scale [7, 14, 29-31]. This

64   method leads to a fast removal of the parent pollutant at pH ~3.0 thanks to the action of $^\bullet OH$

65   formed in the bulk from Fenton's reaction (1), being much slower and usually incomplete the

66   total organic carbon (TOC) abatement due to the accumulation of refractory complexes of

67   Fe(III) with organic intermediates. The mineralization can be upgraded in PEF because UVA

68   light photolyzes most forms of Fe(III) via reactions (3) and (4), thus regenerating Fe^{2+} catalyst

69   [6].

70    $[Fe(OH)]^{2+} + h\nu \rightarrow Fe^{2+} + {}^\bullet OH$ (3)

71    $[Fe(OOCR)]^{2+} + h\nu \rightarrow Fe^{2+} + CO_2 + R^\bullet$ (4)

72   Some authors have attempted to increase the activity and selectivity of H_2O_2 production,

73   reporting the positive contribution of Au-Pd and Pt-Hg nanoparticles [32]. For EF and PEF

74   systems, a few articles discuss the modification of carbonaceous cathodes with non-ferrous

75   metals and the study of their performance at small scale. For example, Pt-Pd nanoparticles were

76   employed to decorate multiwall carbon nanotubes (MWCNTs) supported on reticulated

77   vitreous carbon [33]. Other authors used metallic oxide nanoparticles like Ta_2O_5, $WO_{2.72}$ or

78    $Ce_xA_{1-x}O_2$ (A = Zr, Cu or Ni) immobilized on different substrates [34]. Nevertheless, the most

79   promising and tested materials involve the modification of carbons with Co and Co-based

80   catalysts. For example, CoS_2-based MWCNTs air-diffusion cathodes have been recently

81   developed by our group to degrade the anaesthetic tetracaine [35], showing Co particles the

82   best activity as compared to Cu, Ce, Mn or Fe-modified air-diffusion cathodes [36]. Barros et

83   al. [37] prepared an air-diffusion cathode modified with Co(II) phthalocyanine for the EF

84   treatment of the food dyes Amaranth. Unfortunately, stability tests are rarely addressed, but

85   they are crucial to ensure the continuous reuse of cathodes.

86   The performance assessment of catalyzed cathodes under EF and PEF conditions has been

87   pre-eminently carried out with small volumes of contaminated solutions. Therefore, there is a

88   lack of information on Co-based carbonaceous air-diffusion cathodes at pilot scale. On the other

89   hand, SPEF process constitutes a more viable alternative than PEF to scale-up the technology,

90   since free sunlight replaces expensive UVA lamps yielding much quicker removals

91   [7,14,18,38-42]. However, air-diffusion cathodes employed in SPEF were always uncatalyzed.

92   The combination of catalyzed carbonaceous cathodes with electrocatalytic anodes (M) that

93   foster the production of heterogeneous hydroxyl radical from water oxidation via reaction (5)

94   might enhance the performance of the aforementioned EAOPs, as well as that of electro-

95   oxidation with H_2O_2 production (EO-H_2O_2) in the absence of dissolved iron catalyst [43-45].

96   Among such advanced anodes, boron-doped diamond (BDD) thin films exhibit an outstanding

97   performance, usually better than dimensionally stable metal oxides as RuO_2.

98    $$M + H_2O \rightarrow M(^{\bullet}OH) + H^+ + e^-$$ (5)

99   In this work, the industrial preservative bronopol (2-bromo-2-nitropropane-1,3-diol, $M =$

100   199.989 g mol^{-1}) has been selected as model organic pollutant to test the ability of new Co-

101   based air-diffusion cathodes to generate H_2O_2. As an effective antiseptic, bronopol is ubiquitous

102   in cosmetics, creams and lotions [46]. Lately, important concerns have arisen due to its potential

103   to release formaldehyde, a human carcinogen [47]. On the other hand, aquaculture has grown

104   in recent years thanks to support from European Commission, as a future alternative to

105 decreasing seafood population. Within this context, bronopol is one of the few medicinal

106 products authorized for sea farming in Europe [48]. As a result of their usage, bronopol has

107 been detected even in Arctic environments [49], mainly due to the lack of advanced wastewater

108 treatment facilities [50] as well as the stability of this pollutant against hydrolysis and photolysis

109 [51]. To date, only one article has attempted the treatment of small volumes of bronopol

110 solutions by EF and PEF, using commercial uncatalyzed air-diffusion cathodes [52].

111   Here, MWCNTs decorated with Co-based catalyst in the form of sulfide, very efficient for

112 H_2O_2 production at small scale [35], were prepared as a preliminary step for the subsequent

113 manufacture of air-diffusion cathodes with carbon cloth as substrate. For the first time, this type

114 of cathode has been used to electrogenerate H_2O_2 and treat an organic pollutant like bronopol

115 in 0.050 M Na_2SO_4 at pH 3.0 by EO-H_2O_2, EF, PEF and SPEF using a pre-pilot plant. The

116 experiments were performed with a filter-press flow cell equipped with catalyzed or

117 uncatalyzed cathode and BDD or RuO_2-based anode. The effect of current density (j) and

118 bronopol concentration on its decay kinetics, mineralization, current efficiency and energy

119 consumption was examined, and final carboxylic acids and inorganic ions were quantified.

120 **2. Materials and methods**

121 *2.1. Chemicals*

122   Commercial MWCNTs were supplied by Cheap Tubes Inc. (OD < 8 nm, L 10-30 μm,

123 COOH content 3.86 wt.%). Concentrated sulfuric and nitric acids, cobalt(II) chloride

124 hexahydrate, sodium thiosulfate pentahydrate, sulfur and sodium hypophosphite monohydrate,

125 from Scharlau and Sigma-Aldrich, were of reagent grade. Nafion® perfluorinated resin solution

126 5 wt.% was from Sigma-Aldrich and extra pure 2-propanol from Scharlau. Reagent grade

127 sodium sulfate and iron(II) sulfate heptahydrate (> 98%) were purchased from VWR and

128 Panreac, respectively. Bronopol (98%) was purchased from Sigma-Aldrich. Carboxylic acids

129 and salts used for obtaining the calibration curves were of reagent grade from Merck and

130 Panreac. Ultrapure water from a Millipore Milli-Q system (resistivity > 18.2 MΩ cm) was

131 employed to prepare all the aqueous solutions. Other chemicals were of either HPLC or

132 analytical grade.

133 *2.2. Manufacture of catalysts and air-diffusion cathodes*

134 *2.2.1. Synthesis of catalysts*

135   (Co, S, P)-decorated MWCNTs electrocatalysts (i.e., CoS_xP_y/MWCNTs) were synthesized

136 in two steps. First, CoS_2/MWCNTs were prepared according to Dong et al. [53] by mixing

137 appropriate amounts of $CoCl_2 \cdot 6H_2O$, $Na_2S_2O_3 \cdot 5H_2O$ and S in a PTFE autoclave of 0.25 L

138 capacity, keeping a molar proportion of 2:2:1, with enough quantity of MWCNTs to obtain ca.

139 50 wt.% of nominal Co:S:P in the final sample. About 80% of the total autoclave volume was

140 filled with Milli-Q water and kept at 140 °C for 24 h. Once cooled down, the powder was filtered

141 and washed repeatedly with ultrapure water, ethanol and carbon sulfide. The supported

142 nanoparticles were dried in an air oven at 80 °C. The second step ensured the stabilization of

143 this catalyst by impregnation with a phosphorus precursor followed by thermal treatment. For

144 this, 280 mg of $NaH_2PO_2 \cdot H_2O$ were mixed with 500 mg of fresh CoS_2/MWCNT catalyst, with

145 an atomic ratio Co:S:P of 1:1:1, and treated at 400 °C for 1 h, under argon stream. The CoS_xP_y

146 content in the final supported electrocatalyst was 55 wt.%, corresponding to 27 wt.% Co, 18

147 wt.% S and 10 wt.% P. For comparison, non-decorated MWCNTs were also used in this work.

148 *2.2.2. Manufacture of air-diffusion electrodes*

149   The spraying method was used to manufacture air-diffusion cathodes of 30 cm^2 (6 cm $\times$ 5

150 cm) active geometric area [54]. Unmodified or (Co, S, P)-decorated MWCNTs were

151 ultrasonically dispersed in appropriate amounts of 2-propanol, ultrapure water and Nafion$^{\circledR}$

152 dispersion to form an ink. This ink was sprayed several times onto a carbon cloth with a carbon

153 microporous layer substrate employed as diffusion layer (BASF A7NCV2.1 ELAT$^{\circledR}$ V2.1,

154   thickness 350 μm), using an air-brush gun fed with pure N_2. The material was dried every time

155   in an air oven at 60 ºC for 20 min. The catalyst loading in the CoS_xP_y/MWCNTs air-diffusion

156   electrode was 2.0 mg cm^{-2} and the Nafion® content was 30 wt.% (dry weight).

157   *2.3. H_2O_2 electrogeneration and treatment of bronopol solutions by EAOPs*

158   The pre-pilot plant employed in this study was designed and constructed by us, and a sketch

159   is reported elsewhere [31]. The purpose-made undivided electrochemical filter-press reactor

160   contained a manufactured air-diffusion cathode and either a BDD thin film on a Si wafer or a

161   Ti|RuO_2-based anode. The exposed electrode area was 20 cm^2 (5 cm × 4 cm) and the

162   interelectrode gap was 1.2 cm. Continuous H_2O_2 generation from reaction (2) was ensured by

163   embedding the back side of the cathode in a PVC air chamber fed with pumped air, keeping an

164   overpressure of 8.6 kPa. Electrolyses were run at constant j provided by an N5746A System

165   DC power supply from Agilent Technologies, which also displayed the cell voltage (E_{cell}, see

166   Table S1). In EO-H_2O_2 and EF, light irradiation was prevented by covering the plant with an

167   opaque cloth. In PEF, the flow reactor outlet was connected to an annular glass photoreactor

168   (640 mL of irradiated volume) to illuminate the solution with an Omnilux 27E 160-W UVA

169   lamp (λ_{max} = 360 nm). In SPEF, the photoreactor was a 41°-tilted plane (600 mL of irradiated

170   volume) to collect sunrays perpendicularly, and treatments were carried out in sunny days in

171   August 2018, ensuring a constant UV irradiance (300-400 nm) of ca. 32 W cm^{-2}, as measured

172   on a Kipp & Zonen CUV 5 radiometer.

173   H_2O_2 electrogeneration trials and bronopol treatments were made in 0.050 M Na_2SO_4 at

174   pH 3.0, the optimum value for Fenton's reaction (1) [6]. In EF, PEF and SPEF, 0.50 mM of

175   Fe^{2+} catalyst was chosen for sufficient •OH production, as was found in systems with air-

176   diffusion cathodes [28,31]. The surface of each fresh cathode was activated by electrolyzing a

177   0.050 M Na_2SO_4 solution at pH 3.0 and 35 ºC with a RuO_2-based anode at 25 mA cm^{-2}. After

178   three consecutive runs of 360 min each, reproducible H_2O_2 profiles were obtained. The good

179 stability of the (Co, S, P)-catalyzed cathodes was assessed from Co leaching. All the

180 experiments with catalyzed cathodes were carried out in duplicate with only two different

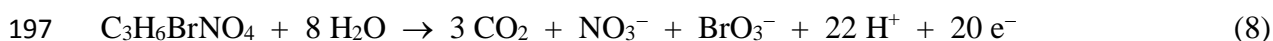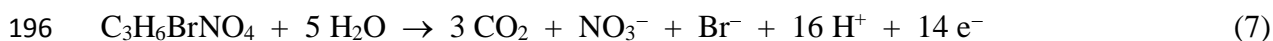181 pieces, one for electrogeneration trials and another one for bronopol treatments.

182 *2.4. Apparatus and analytical methods*

183 The pH of each solution was adjusted before current supply using a Crison 2000 pH-meter.

184 The accumulated H_2O_2 was determined by the metavanadate method using a Shimadzu 1800

185 UV/Vis spectrophotometer at $\lambda = 450$ nm [55]. The current efficiency for H_2O_2

186 electrogeneration was calculated as proposed elsewhere [6].

187 The solution TOC was determined on a Shimadzu VCSN TOC analyzer after filtration with

188 0.45 µm Whatman PTFE filters. The mineralization current efficiency (MCE) upon treatment

189 of V_s at constant current I (A) during electrolysis time t (h) was then estimated as follows [6]:

190 $$\% \ \mathrm{MCE} = \frac{n \, F \, V_s \, \triangle(\mathrm{TOC})_{exp}}{4.32 \times 10^7 \, m \, I \, t} \times 100 \tag{6}$$

191 where F is the Faraday constant (96,487 C mol^{-1}), $\triangle(\mathrm{TOC})_{exp}$ is the determined TOC removal

192 (mg L^{-1}), 4.32×10^7 is a conversion factor and $m = 3$ is the number of carbon atoms of bronopol.

193 Considering the pollutant mineralization to CO_2, NO_3^- and Br^- (using the RuO_2-based anode)

194 or BrO_3^- (using BDD), as will be discussed below, the number n of electrons for the theoretical

195 total mineralization was taken as 14 from Eq. (7) or 20 from Eq. (8):

196 $$C_3H_6BrNO_4 + 5\,H_2O \rightarrow 3\,CO_2 + NO_3^- + Br^- + 16\,H^+ + 14\,e^- \tag{7}$$

197 $$C_3H_6BrNO_4 + 8\,H_2O \rightarrow 3\,CO_2 + NO_3^- + BrO_3^- + 22\,H^+ + 20\,e^- \tag{8}$$

198 The specific energy consumption per unit TOC mass (EC_{TOC}, kWh (g TOC)$^{-1}$) during the

199 same degradaion trials was calculated from E_{cell} values as suggested elsewhere [6].

200 Bronopol concentration decay was monitored by reversed-phase high-performance liquid

201 chromatography (HPLC) using a Waters 600 chromatograph, with a BDS Hypersil C18 6 µm

202   (250 mm × 4.6 mm) column at 35 ºC, coupled to a Waters 996 photodiode array at $\lambda = 211$ nm.

203   The mobile phase was a 50:50 (v/v) acetonitrile/water (10 mM KH_2PO_4 at pH 3.0) mixture at

204   0.8 mL min^{-1}. All fresh samples were immediately diluted with acetonitrile to stop the

205   degradation. The chromatograms displayed the peak of bronopol at retention time (t_r) of 4.2

206   min, with limits of quantification (LOQ) and detection (LOD) of 0.530 and 0.158 mg L^{-1},

207   respectively. Final carboxylic acids were quantified by ion-exclusion HPLC with the above

208   liquid chromatograph, as reported in earlier work [41]. These chromatograms only displayed

209   one peak associated with formic acid at $t_r = 13.9$ min.

210   Concentrations of BrO_3^-, Br^- and NO_3^- released during bronopol treatment were measured

211   by ion chromatography [52]. Peaks were found at 2.3, 3.4 and 4.0 min, respectively. NH_4^+

212   content was measured according to the standard indophenol blue reaction [14]. The leached

213   cobalt from catalyzed cathodes was determined by inductively coupled plasma-optical emission

214   spectrometry (ICP-OES) on a Perkin Elmer Optima 3200 L spectrometer.

215   **3. Results and discussion**

216   *3.1. H_2O_2 electrogeneration with catalyzed and uncatalyzed cathodes*

217   Fig. 1a shows the H_2O_2 accumulation with time in the pre-pilot plant upon O_2 reduction on

218   catalyzed and uncatalyzed cathodes at 40 mA cm^{-2}. The enhanced electrogeneration ability of

219   the (Co, S, P)-decorated MWCNTs air-diffusion cathode was verified in all EAOPs tested,

220   yielding 15.9, 7.4 and 3.5 mM H_2O_2 after 360 min of EO-H_2O_2, EF and PEF, respectively,

221   instead of 9.5, 4.7 and 0.9 mM achieved with the unmodified MWCNTs cathode. This is in

222   agreement with the good results obtained with Co-based cathodes at smaller scale [36]. The

223   lower accumulation in EF as compared to EO-H_2O_2 demonstrates the occurrence of Fenton's

224   reaction (1) in the presence of 0.50 mM Fe^{2+}, thus ensuring a continuous source of •OH. The

225   conversion of H_2O_2 into •OH was accelerated in PEF, owing to the photoregeneration of Fe^{2+}

under UVA irradiation, according to photo-Fenton reaction (3). Note that, in all cases, the profiles tended to reach a plateau, which resulted from the use of an undivided filter-press cell, where H_2O_2 was partially oxidized at the RuO_2 anode. Upon prolonged electrolysis, the decomposition rate tended to equate its electrogeneration rate at the catalyzed air-diffusion cathode [6].

The effect of j on H_2O_2 concentration was assessed for the three EAOPs under the same electrolytic conditions reported in Fig. 1a. As shown in Fig. 1b, the H_2O_2 accumulated at 360 min decreased to 11.3 and 4.0 mM in EO-H_2O_2 process at j of 25 and 10 mA cm^{-2}, respectively. This trend was expected since feeding of reagents required for reaction (2) is ensured and hence, the H_2O_2 production was uniquely dependent on the electron supply and can be effectively dosed by simply modulating the input current. However, Fig. 1c shows that the efficiency at 30 min decreased in the sequence 100% > 85% > 72%, when j was raised from 10 to 40 mA cm^{-2}. At the lowest j, O_2 was only reduced to H_2O_2, whereas the competitive four-electron reduction to H_2O occurred to a gradually larger extent at a higher j, due to the change of the cathode potential to more negative values. As seen in Fig. 1c, the current efficiency underwent a progressive decay, which is not surprising because of the simultaneous oxidation of H_2O_2 at the anode surface and its cathodic reduction, as well as its chemical decomposition in the bulk. These destruction reactions justify that, at 360 min, a similar efficiency of 51-54% was obtained at all j values.

A similar effect of j on the time course of H_2O_2 was observed in EF (Fig. S1a) and PEF (Fig. S1b) processes. Note that, in both systems, the increase of j stimulated all aforementioned parasitic reactions, and also accelerated the Fe^{2+} regeneration from Fe^{3+} reduction at the cathode, thus favoring the H_2O_2 consumption by Fenton's reaction (1). However, the inherent upgrade in H_2O_2 electrogeneration at 25 and 40 mA cm^{-2} counteracted all these side reactions, eventually ending in a greater H_2O_2 accumulation in the order: $10 < 25 < 40$ mA cm^{-2}.

251   The electrogeneration performance of the catalyzed and uncatalyzed cathodes was also

252 compared using an undivided electrochemical reactor equipped with a BDD anode. Fig. S2

253 shows that under PEF conditions at 40 mA cm^{-2}, a much greater H_2O_2 accumulation was

254 achieved again for the Co-based air-diffusion electrode, reaching 3.5 mM instead of 0.6 mM.

255 Note that there was no difference in H_2O_2 accumulation between the RuO_2/air-diffusion (Fig.

256 1a) and BDD/air-diffusion cells, which means that in Fenton-based processes, the H_2O_2 was

257 mainly destroyed via Fenton's reaction (1), which was predominant over its anodic destruction.

258   The stability of the (Co, S, P)-decorated MWCNTs air-diffusion cathodes with a large

259 surface area (20 cm^2 in contact with the solution) is a crucial feature for their further

260 implementation. This was assessed by monitoring Co leaching during the activation of fresh

261 catalyzed cathodes, which revealed the accumulation of 0.68-0.99 mg L^{-1} during the first run,

262 yielding undetectable traces below LOD (0.02 mg L^{-1}) in successive electrogeneration trials.

263 Considering the catalyst composition and loading (sections 2.2.1 and 2.2.2), 10.8 mg Co were

264 exposed to the solution during the first activation, with a Co loose of 9% as maximal. On the

265 other hand, Fig. S3 shows the images of the catalyzed cathode before and after activation under

266 PEF conditions, using either a RuO_2-based or BDD anode. It can be observed that the central

267 region, which contained the electrocatalytic coating, maintained its complete uniformity, with

268 only some additional $Fe(OH)_3$ deposition, as typically occurs during Fenton-based

269 electrochemical treatments. The large stability of the cathode allowed a good reproducibility

270 upon successive trials, losing less than 1% efficiency after more than 20 electrogeneration runs.

271 *3.2. Treatment of bronopol solutions by EAOPs*

272   Fig. 2a shows the decay of bronopol content during PEF treatment of solutions with 0.28

273 mM (10 mg L^{-1} TOC) using a RuO_2-based anode at 40 mA cm^{-2}. It was completely removed

274 after 360 min employing the catalyzed cathode, whereas 5% of pollutant was still present using

275 the uncatalyzed cathode. This different behavior confirms that the higher H_2O_2 accumulation

276 shown in Fig. 1a using the former cathode leads to a faster generation of $^\bullet$OH from Fenton's

277 reaction (1). Worth mentioning, bronopol was much more resistant than aromatic organic

278 pollutants degraded by PEF at pre-pilot scale, whose complete removal is typically achieved in

279 only few minutes. For example, less than 18 min were required to remove 0.174 mM naproxen

280 at 50 mA cm^{-2} under similar condition [30].

281   In both PEF systems, bronopol concentration decay obeyed a pseudo-first-order kinetics

282 (Fig. 2b), which is coherent with the generation of a constant amount of reactive $^\bullet$OH as the

283 main oxidant species. As expected, a significantly greater rate constant (k_{app}) resulted from the

284 electrolysis with the catalyzed cathode, i.e., 0.015 vs 0.009 min^{-1}. The mineralization of the

285 same bronopol solutions followed the same trend, with Fig. 2c revealing a higher TOC removal

286 (77% vs 64% at 360 min) when the electrochemical reactor was equipped with the Co-based

287 cathode.

288   The performance of the catalyzed air-diffusion cathode under PEF conditions was

289 compared with that observed in EO-H$_2$O$_2$ and EF. As shown in Fig. 3a, bronopol removal at

290 360 min was 44%, 92% and 100% in EO-H$_2$O$_2$, EF and PEF. All the decays agreed with a

291 pseudo-first-order reaction kinetics, as highlighted in Fig. 3b, yielding k_{app} values of 0.002,

292 0.007 and 0.014 min^{-1}, respectively ($R^2 > 0.98$). The superiority of EF and PEF over EO-H$_2$O$_2$

293 arises from the abundance of $^\bullet$OH produced in the bulk from Fenton's reaction (1), which are

294 much more effective than both, direct anodic oxidation on the anode surface and mediated

295 oxidation by RuO$_2$($^\bullet$OH). PEF was the most powerful treatment thanks to the continuous Fe^{2+}

296 regeneration from reaction (3), which resulted in a larger production of $^\bullet$OH during the run.

297 Note that this effect has been rarely observed during the treatment of less refractory pollutants,

298 since the photolytic action of UVA light requires long reaction times that are not commonly

299 needed by aromatic molecules, in contrast to the current aliphatic contaminant.

300   TOC removal during the application of the same three EAOPs is depicted in Fig. 3c. No

301   mineralization was achieved in EO-H_2O_2, thus confirming the small oxidation power of

302    $RuO_2(^\bullet OH)$. In contrast, up to 52% TOC abatement was attained after 360 min of EF, which

303   resulted from the progressive combustion of many degradation by-products by $^\bullet OH$. However,

304   many of them became quite refractory and could only undergo a slow destruction upon

305   irradiation with UVA light, which photodecomposed some of the complexes formed between

306   Fe(III) and organic aliphatic by-products. The slow and only partial TOC removal yielded a

307   very low MCE, always below 8%. The highest mineralization current efficiency along with the

308   corresponding lowest EC_{TOC}, calculated from cell voltage values given in Table S1, were found

309   for PEF treatment (Fig. 3d and 3e).

310   The effect of j on the performance of PEF treatment with the RuO_2-based anode and

311   catalyzed cathode can be seen in Fig. S4. As expected from the lower H_2O_2 accumulation (Fig.

312   S1b), bronopol removal was slower at 25 mA cm^{-2} (96%) and 10 mA cm^{-2} (85%) as compared

313   to PEF at 40 mA cm^{-2}, yielding k_{app} values of 0.010 and 0.005 min^{-1} ($R^2 \geq 0.99$). Similarly,

314   smaller TOC decays (72% and 56%, respectively) were attained. However, gradually higher

315   MCE and lower energy consumption values resulted when j decreased from 40 to 10 mA cm^{-2},

316   which can be explained by the excessive number of parasitic reactions that appear as the applied

317   current is increased [6,8]

318   The effect of initial bronopol concentration on the same PEF treatment at 40 mA cm^{-2} was

319   also investigated, trying to assess the feasibility of treating highly polluted solutions by the most

320   powerful EAOP. In Fig. S5a, trials with 0.28, 0.56 and 0.84 mM bronopol are compared. Total

321   degradation was not possible for solutions with > 0.28 mM, attaining removals of 88% as

322   maximum at 360 min. The decays still obeyed a pseudo-first-order kinetics, although with

323   smaller k_{app} values of 0.006 min^{-1}. This deceleration at too high pollutant contents was

324   confirmed from the time course of TOC (Fig. S5c), which was removed by 52% and 44% for

325   0.56 and 0.84 mM bronopol, thus suggesting that the number of accumulated $^\bullet$OH at 40 mA

326   cm^{-2} was insufficient to reach a faster mineralization. Typically, the presence of a large amount

327   of organic matter enhances the MCE of EAOPs, owing to the minimization of parasitic

328   reactions involving the $^\bullet$OH. However, the slow TOC removal at high bronopol concentration

329   prevented obtaining high MCE values (Fig. S5d). Similarly, lower energy consumptions per

330   unit TOC mass, as compared to PEF at 40 mA cm^{-2}, could not be attained (Fig. S5e).

331   Aiming to enhance the performance of PEF treatment with the catalyzed cathode at 40 mA

332   cm^{-2}, the RuO$_2$-based anode was replaced by BDD. The influence of the anode nature was

333   dramatic in EO-H$_2$O$_2$ since it yielded bronopol and TOC removals of 91% (Fig. 4a) and 58%

334   (Fig. 4c) at 360 min using BDD instead of 44% and 0% reached with RuO$_2$-based anode. These

335   results arise from the high oxidation power of BDD($^\bullet$OH), which was accumulated with a

336   constant concentration that led to a pseudo-first-order kinetics with $k_{app} = 0.007$ min^{-1} (Fig. 4b).

337   In contrast, the anode had a less significant role in PEF, showing almost no difference in

338   bronopol removal due to the superior contribution of $^\bullet$OH in the bulk (Fig. 4a). However, BDD

339   exhibited a positive effect as for TOC abatement, since the reaction of BDD($^\bullet$OH) with very

340   stable by-products and their Fe(III) complexes favored the quicker mineralization, attaining

341   91% instead of 77% (Fig. 4c).

342   *3.3. Detection of final carboxylic acids and fate of inorganic ions*

343   The intensive action of $^\bullet$OH and M($^\bullet$OH) on aromatic and aliphatic pollutants usually

344   causes the accumulation of short-chain aliphatic carboxylic acids, which account for by the high

345   refractoriness of solution TOC during the last stages of EAOPs. In the present work, formic

346   acid was identified as the main degradation by-product by ion-exclusion HPLC, in agreement

347   with that observed in our previous study [52]. Fig. 5a shows the concentration profiles of this

348   acid in the three EAOPs tested, with the RuO$_2$-based anode and catalyzed cathode, at 40 mA

349   cm^{-2}. The concentration gradually increased in EO-H$_2$O$_2$ and EF, attaining 10-13 mg L^{-1} at 360

350 min, whereas it was completely destroyed in PEF, thus justifying the larger TOC removal

351 attained in it (Fig. 3c). Fig. S6a highlights a difference between solution TOC and (bronopol +

352 formic acid) equivalent TOC at each time, which can be related with the accumulation of

353 unidentified organic by-products. Fig. 5b evidences that the treatment of more concentrated

354 bronopol solutions by PEF involved a larger accumulation of formic acid, which was very

355 refractory and remained in the final solutions, in agreement with the large TOC amount at 360

356 min shown in Fig. S5c. Again, Fig. S6b informs about the existence of unidentified by-products.

357   Several electrolyses were performed with the catalyzed cathode to determine the inorganic

358 ions released from the heteroatoms contained in solutions with 0.56 mM bronopol. Fig. 6a

359 shows the time course of ions in EO-H_2O_2 and PEF with a RuO_2-based anode. In the former

360 treatment, 0.11 mM Br^- and 0.11 mM NO_3^- were accumulated at 360 min, along with half of

361 the initial concentration of bronopol, whereas 0.30 mM Br^- and 0.36 mM NO_3^- were released

362 in PEF. This means that some brominated and nitrogenated molecules were also formed,

363 accounting for by the undetected Br and N content, since neither BrO_3^- nor NO_2^- appeared in

364 the chromatograms and less than 1 mg L^{-1} NH_4^+ was found. Based on the conclusions from Fig.

365 S6a and S6b, the undetected molecules corresponded to organic compounds, as for example

366 bromonitromethane [52]. Fig. 6b and c illustrate the results obtained for brominated and

367 nitrogenated ions by analogous trials with BDD anode, respectively. Also in these cases, some

368 organic by-products containing Br and N were plausibly formed, being the main difference the

369 progressive transformation of Br^- into BrO_3^- upon attack of $^\bullet OH$ and $M(^\bullet OH)$ [5].

370 *3.4. Solar photoelectro-Fenton treatment*

371   Since PEF showed the best performance among all EAOPs, the possibility of using sunlight

372 as an inexpensive irradiation source was explored. Fig. 7 shows the performance of SPEF

373 treatments of 0.28 mM bronopol solutions with either a RuO_2-based or BDD anode at $j = 40$

374 mA cm^{-2}. Total bronopol removal was achieved at 360 and 300 min using the RuO_2-based anode

and the catalyzed or uncatalyzed cathode, respectively (Fig. 7a). This confirms the enhanced degradation with the Co-based cathode, as well as the aimed superiority of SPEF over PEF (Fig. 2a) thanks to the greater photon flux and the contribution of visible photons of sunlight. The corresponding k_{app} values were 0.012 and 0.016 min^{-1} (Fig. 7b). These findings were verified with the BDD anode, which allowed the complete destruction after 300 and 210 min (k_{app} of 0.018 and 0.021 min^{-1}), quicker than PEF (Fig. 4a). SPEF treatment with the BDD anode and catalyzed air-diffusion cathode was the best among all EAOPs, yielding a greater mineralization of 94% at 360 min (Fig. 7c) as compared to PEF (Fig. 4c) and giving rise to the highest MCE values of this study (Fig. 7d). The replacement of BDD by the less expensive RuO_2-based anode led to a TOC removal of 88%, exhibiting a lower energy consumption (Fig. 7e) due to the decrease in E_{cell}.

4. Conclusions

This work has demonstrated that Co-based air-diffusion cathodes enhance the electrocatalytic H_2O_2 production as compared to uncatalyzed ones, reaching up to 100% current efficiency at low j. These cathodes showed a good stability during prolonged electrolyses, showing a small Co release into treated solutions. The great H_2O_2 generation served to produce $^{\bullet}OH$ from Fenton's reaction in the presence of 0.50 mM Fe^{2+}. As a result, complete removal of bronopol with a large percentage of mineralization was achieved, with performance increasing in the sequence: EO-H_2O_2 < EF < PEF < SPEF. BDD was superior to the RuO_2-based anode due to the higher oxidation power of BDD($^{\bullet}OH$) as compared to RuO_2($^{\bullet}OH$). Bronopol was mainly transformed into formic acid as final by-product, although the formation of some other organic intermediate with Br and N atoms was also deduced from the accumulation profiles of Br^-, BrO_3^- and NO_3^- ions.

398 **Acknowledgements**

404 **References**

405 [1]   J.M. Campos-Martín, G. Blanco-Brieva, J.L. Fierro, Angew. Chem. Int. Ed. 45 (2006)

406   6962-6984.

407 [2]   ReportLinker, 2018 Future of global hydrogen peroxide market to 2025- Growth

408   opportunities, competition, trends and outlook of hydrogen peroxide across applications

409   and regions report. https://www.reportlinker.com/p05505747/Future-of-Global-

410   Hydrogen-Peroxide-Market-to-Growth-Opportunities-Competition-Trends-and-

411   Outlook-of-Hydrogen-Peroxide-Across-Applications-and-Regions-Report.html, 2018

412   (accessed 24 September 2018).

413 [3]   S. Yang, A. Verdaguer-Casadevall, L. Arnarson, L. Silvioli, V. Čolić, R. Frydendal, J.

414   Rossmeisl, Ib Chorkendorff, I.E.L. Stephens, ACS Catal. 8 (2018) 4064-4081.

415 [4]   M.A. Oturan, J.-J. Aaron, Crit. Rev. Environ. Sci. Technol. 44 (2014) 2577-2641.

416 [5]   I. Sirés, E. Brillas, M.A. Oturan, M.A. Rodrigo, M. Panizza, Environ. Sci. Pollut. Res. 21

417   (2014) 8336-8367.

418 [6]   E. Brillas, I. Sirés, M.A. Oturan, Chem. Rev. 109 (2009) 6570-661.

419 [7]   E. Brillas, J. Braz. Chem. Soc. 25 (2014) 393-417.

420 [8]   M. Zhou, M.A. Oturan, I. Sirés, Electro-Fenton Process – New Trends and Scale-Up, The

421   Handbook of Environmental Chemistry, vol. 61, Springer Nature, Singapore, 2018.

422   [9]   A. Ashgar, A.A.A. Raman, W.M.A.W. Daud, M. Ahmad, S.U.B.M. Zain, J. Taiwan Inst.

423   Chem. Eng. 76 (2017) 89-100.

424   [10]   M. Panizza, M.A. Oturan, Electrochim. Acta 56 (2011) 7084-7087.

425   [11]   G. Coria, T. Pérez, I. Sirés, J. L. Nava, J. Electroanal. Chem. 757 (2015) 225-229.

426   [12]   O. Ganzenko, N. Oturan, I. Sirés, D. Huguenot, E.D. van Hullebusch, G. Esposito, M.A.

427   Oturan, Environ. Chem. Lett. 16 (2018) 281-286.

428   [13]   H.C. Arredondo Valdez, G. García Jiménez, S. Gutiérrez Granados, C. Ponce de León,

429   Chemosphere 89 (2012) 1195-1201.

430   [14]   A. Thiam, I. Sirés, F. Centellas, P.L. Cabot, E. Brillas, Chemosphere 136 (2015) 1-8.

431   [15]   X. Yu, M. Zhou, G. Ren, L. Ma, Chem. Eng. J. 263 (2015) 92-100.

432   [16]   A. Galia, S. Lanzalaco, M.A. Sabatino, C. Dispenza, O. Scialdone, I. Sirés, Electrochem.

433   Commun. 62 (2016) 64-68.

434   [17]   Y. Lu, G. Liu, H. Luo, R. Zhang, Electrochim. Acta 248 (2017) 29-36.

435   [18]   G. Coria, T. Pérez, I. Sirés, E. Brillas, J.L. Nava, Chemosphere 198 (2018) 174-181.

436   [19]   T. Pérez, G. Coria, I. Sirés, J.L. Nava, A.R. Uribe, J. Electroanal. Chem. 812 (2018) 54-

437   58.

438   [20]   J.F. Pérez, J. Llanos, C. Sáez, C. López, P. Cañizares, M.A. Rodrigo, Electrochem.

439   Commun. 71 (2016) 65-68.

440   [21]   O. Scialdone, A. Galia, C. Gattuso, S. Sabatino, B. Schiavo, Electrochim. Acta 182 (2015)

441   775-780.

442   [22]   K.V. Plakas, A.J. Karabelas, S.D. Sklari, V.T. Zaspalis, Ind. Eng. Chem. Res. 52 (2013)

443   13948-13956.

444   [23]   H. Roth, Y. Gendel, P. Buzatu, O. David, M. Wessling, J. Hazard. Mater. 307 (2016) 1-

445   6.

446   [24]   F. Yu, Y. Chen, H. Ma, New J. Chem. 42 (2018) 4485-4494.

447   [25] T.X.H. Le, M. Bechelany, S. Lacour, N. Oturan, M.A. Oturan, M. Cretin, Carbon 94
448   (2015) 1003-1011.

449   [26] E. Mousset, Z. Wang, J. Hammaker, O. Lefebvre, Electrochim. Acta 214 (2016) 217-230.

450   [27] W. Yang, M. Zhou, J. Cai, L. Liang, G. Ren, L. Jiang, J. Mater. Chem. A 5 (2017) 8070-
451   8080.

452   [28] J.C. Murillo-Sierra, I. Sirés, E. Brillas, E.J. Ruiz-Ruiz, A. Hernández-Ramírez,
453   Chemosphere 192 (2018) 225-233.

454   [29] G.R. Agladze, G.S. Tsurtsumia, B.-I. Jung, J.-S. Kim, G. Gorelishvili, J. Appl.
455   Electrochem. 37 (2007) 375-383.

456   [30] G. Coria, I. Sirés, E. Brillas, J.L. Nava, Chem. Eng. J. 304 (2016) 817-825.

457   [31] A. Thiam, R. Salazar, E. Brillas, I. Sirés, Chem. Eng. J. 335 (2018) 133-144.

458   [32] A. Verdaguer-Casadevall, D. Deiana, M. Karamad, S. Siahrostami, P. Malacrida, T.W.
459   Hansen, J. Rossmeisl, I. Chorkendorff, I.E.L. Stephens, Nano Lett. 14 (2014) 1603-1608.

460   [33] R.M. Félix-Navarro, M. Beltrán-Gastélum, M.I. Salazar-Gastélum, C. Silva-Carrillo,
461   E.A. Reynoso-Soto, S. Pérez-Sicarios, S.W. Lin, F. Paraguay-Delgado, G. Alonso-
462   Núñez, J Nanopart Res 15:1802 (11 pages).

463   [34] E.C. Paz, L.R. Aveiro, V.S. Pinheiro, F.M. Souza, V.B. Lima, F.L. Silva, P. Hammer,
464   M.R.V. Lanza, M.C.S. Santos, Appl. Catal. B: Environ. 232 (2018) 436-445.

465   [35] C. Ridruejo, F. Alcaide, G. Álvarez, E. Brillas, I. Sirés, J. Electroanal. Chem. 808 (2018)
466   364-371.

467   [36] L. Liang, Y. An, M. Zhou, F. Yu, M. Liu, G. Ren, J. Environ. Chem. Eng. 4 (2016) 4400-
468   4408.

469   [37] W.R.P. Barros, P.C. Franco, J.R. Steter, R.S. Rocha, M.R.V. Lanza, J. Electroanal. Chem.
470   722-723 (2014) 46-53.

471   [38] C. Espinoza, J. Romero, L. Villegas, L. Cornejo-Ponce, R. Salazar, J. Hazard. Mater. 319

472   (2016) 24-33.

473   [39] F. Gozzi, I. Sirés, A. Thiam, S.C. de Oliveira, A. Machulek Jr., E. Brillas, Chem. Eng. J.

474   310 (2017) 503-513.

475   [40] T. Pérez, I. Sirés, E. Brillas, J.L. Nava, Electrochim. Acta 228 (2017) 45-56.

476   [41] J.R. Steter, E. Brillas, I. Sirés, Appl. Catal. B: Environ. 224 (2018) 410-418.

477   [42] I. Salmerón, K. Plakas, I. Sirés, I. Oller, M.I. Maldonado, A.J. Karabelas, S. Malato, Appl.

478   Catal. B: Environ. https://doi:10.1016/j.apcatb.2018.09.045

479   [43] B. Marselli, J. García-Gomez, P.A. Michaud, M.A. Rodrigo, C. Comninellis, J.

480   Electrochem. Soc. 150 (2003) D79-D83.

481   [44] M. Panizza, G. Cerisola, Chem. Rev. 109 (2009) 6541-6569.

482   [45] C.A. Martínez-Huitle, M. Panizza, Curr. Opin. Electrochem. (2018), doi:

483   https://doi.org/10.1016/j.coelec.2018.07.010.

484   [46] M.A. Pastor-Nieto, F. Alcántara-Nicolás, V. Melgar-Molero, R. Pérez-Mesonero, A.

485   Vergara-Sánchez, A. Martín-Fuentes, P. González-Muñoz, E. de Eusebio-Murillo, Actas

486   Dermosifiliog. 108 (2017) 758-770.

487   [47] M. Kireche, J.-L. Peiffer, D. Antonios, I. Fabre, E. Giménez-Arnau, M. Pallardy, J.-P.

488   Lepoittevin, J.-C. Ourlin, Chem. Res. Toxicol. 24 (2011) 2115-2128.

489   [48] V. Tornero, G. Hanke, Marine Pollut. Bull. 112 (1-2) (2016) 17-38.

490   [49] C. Dye, M. Schlabach, J. Green, M. Remberger, L. Kaj, A. Palm, Bronopol, resorcinol,

491   m-cresol and triclosan in the Nordic environment, in: B. Bürgel Mogensen, M.J.P.H.

492   Dam, J.A.S.S. Mannio, O.B.H. Glesne, K. Suomalainen (Eds.), Thema North, Nordic

493   Screen reports, Nordic Council of Ministers, Copenhagen, 2007.

494   [50] R. Kallenborn, E. Brorström-Lundén, L.O. Reiersen, S. Wilson, Environ. Sci. Pollut. Res.

495   https://doi 10.1007/s11356-017-9726-6).

496   [51]   M. Matczuk, N. Obarski, M. Mojski, Int. J. Cosmet. Sci. 34 (2012) 451-457.

497   [52]   E. Bocos, E. Brillas, M.A. Sanromán, I. Sirés, Environ. Sci. Technol. 50 (2016) 7679-

498   7686.

499   [53]   J. Dong, D. Li, Z. Peng, Y. Zhou, Synthesis and electrochemical performance of cobalt

500   disulfide, J. Solid State Electrochem. 12 (2008) 171-174.

501   [54]   G. Álvarez, F. Alcaide, P.L. Cabot, M.J. Lázaro, E. Pastor, J. Solla-Gullón, Int. J. Hydrog.

502   Energy 37 (2012) 393–404.

503   [55]   R.F. Pupo Nogueira, M.C. Oliveira, W.C. Paterlini, Talanta 66 (2005) 86-91.

504

Figure captions

Fig. 1. (a) Time course of H_2O_2 concentration accumulated in 2.5 L of 0.050 M Na_2SO_4 at pH

3.0 and 35 °C using a filter-press reactor with a RuO_2-based anode and: (●,■,▲) (Co, S, P)-

modified and (○,□,△) uncatalyzed MWCNTs air-diffusion cathodes. EAOP: (●,○) EO-H_2O_2

(■,□) EF with 0.50 mM Fe^{2+} and (▲,△) PEF with 0.50 mM Fe^{2+} and 160-W UVA lamp.

Current density (j) of 40 mA cm^{-2} and liquid flow rate of 180 L h^{-1}. (b) Accumulated H_2O_2

concentration vs. electrolysis time under the above EO-H_2O_2 conditions using a (Co, S, P)-

modified air-diffusion cathode at j: (◆) 10 mA cm^{-2}, (▼) 25 mA cm^{-2} and (●) 40 mA cm^{-2}. (c)

Current efficiency during these trials.

Fig. 2. Normalized (a) bronopol concentration and (c) TOC decays with electrolysis time during

the PEF treatment of 2.5 L of 0.28 mM bronopol (10 mg L^{-1} TOC) solutions in 0.050 M Na_2SO_4

with 0.50 mM Fe^{2+} at pH 3.0 and 35 ºC using a filter-press reactor with a RuO_2-based anode

and (▲) (Co, S, P)-modified or (△) uncatalyzed MWCNTs air-diffusion cathode at $j = 40$ mA

cm^{-2} and liquid flow rate of 180 L h^{-1}. (b) Pseudo-first-order kinetic analysis for data of plot (a).

Fig. 3. (a) Normalized bronopol concentration removal vs. time and (b) corresponding pseudo-

first-order kinetic analysis, (c) normalized TOC decay with electrolysis time and corresponding

(c) mineralization current efficiency and (d) specific energy consumption per unit TOC mass

during the treatment of 2.5 L of 0.28 mM bronopol solutions with 0.050 M Na_2SO_4 at pH 3.0

and 35 ºC by (●) EO-H_2O_2, (■) EF with 0.50 mM Fe^{2+} and (▲) PEF with 0.50 mM Fe^{2+}

employing a RuO_2-based anode and (Co, S, P)-modified MWCNTs air-diffusion cathode at $j = $

40 mA cm^{-2} and liquid flow rate of 180 L h^{-1}.

Fig. 4. (a) Normalized bronopol concentration removal with time, (b) corresponding pseudo-

first-order kinetic analysis and (c) normalized TOC decay with time during the (●,○) EO-H_2O_2

and (▲,△) PEF treatments of 0.28 mM bronopol solutions under the same conditions of Fig.

529   3 using a (●,▲) RuO$_2$-based or (○,△) BDD anode and (Co, S, P)-modified MWCNTs air-

530   diffusion cathode.

531   **Fig. 5.** (a) Time course of formic acid formed during the (●) EO-H$_2$O$_2$, (■) EF and (▲) PEF

532   treatments of the 0.28 mM bronopol (10 mg L^{-1} TOC) solutions shown in Fig. 3. (b) Formic

533   acid accumulation profiles during the PEF treatment under the conditions shown in plot (a), at:

534   (▼) 0.56 mM (20 mg L^{-1} TOC) and (◆) 0.84 mM (30 mg L^{-1} TOC) bronopol.

535   **Fig. 6.** (a) Evolution of the concentration of (○,●) Br$^-$ and (□,■) NO$_3^-$ released and (△)

536   bronopol removed during the (○,□,△) EO-H$_2$O$_2$ and (●,■) PEF (with 0.50 mM Fe^{2+})

537   treatments of 2.5 L of 0.56 mM (20 mg L^{-1} TOC) bronopol in 0.020 M Na$_2$SO$_4$ at pH 3.0 and

538   35 ℃ using a RuO$_2$-based anode and (Co, S, P)-modified MWCNTs air-diffusion cathode at j

539   = 20 mA cm^{-2} and liquid flow rate of 180 L h^{-1}. (b) Evolution of the concentration of (○,●)

540   Br$^-$, (◇,◆) BrO$_3^-$, (▽,▼) sum of Br$^-$ + BrO$_3^-$ and (c) (□,■) NO$_3^-$ released during the

541   (○,◇,▽,□) EO-H$_2$O$_2$ and (●,◆,▼,■) PEF treatments under the same conditions, but using

542   a BDD anode.

543   **Fig. 7.** (a) Normalized bronopol concentration removal vs. time and (b) corresponding pseudo-

544   first-order kinetic analysis, (c) normalized TOC decay with electrolysis time and corresponding

545   (c) mineralization current efficiency and (d) specific energy consumption per unit TOC mass

546   during the SPEF treatment of 2.5 L of 0.28 mM bronopol solutions in 0.050 M Na$_2$SO$_4$ with

547   0.50 mM Fe^{2+} at pH 3.0 and 35 ℃ using a (○,●) RuO$_2$-based or (□,■) BDD anode and (○,□)

548   uncatalyzed or (●,■) (Co, S, P)-modified MWCNTs air-diffusion cathode at j = 40 mA cm^{-2}
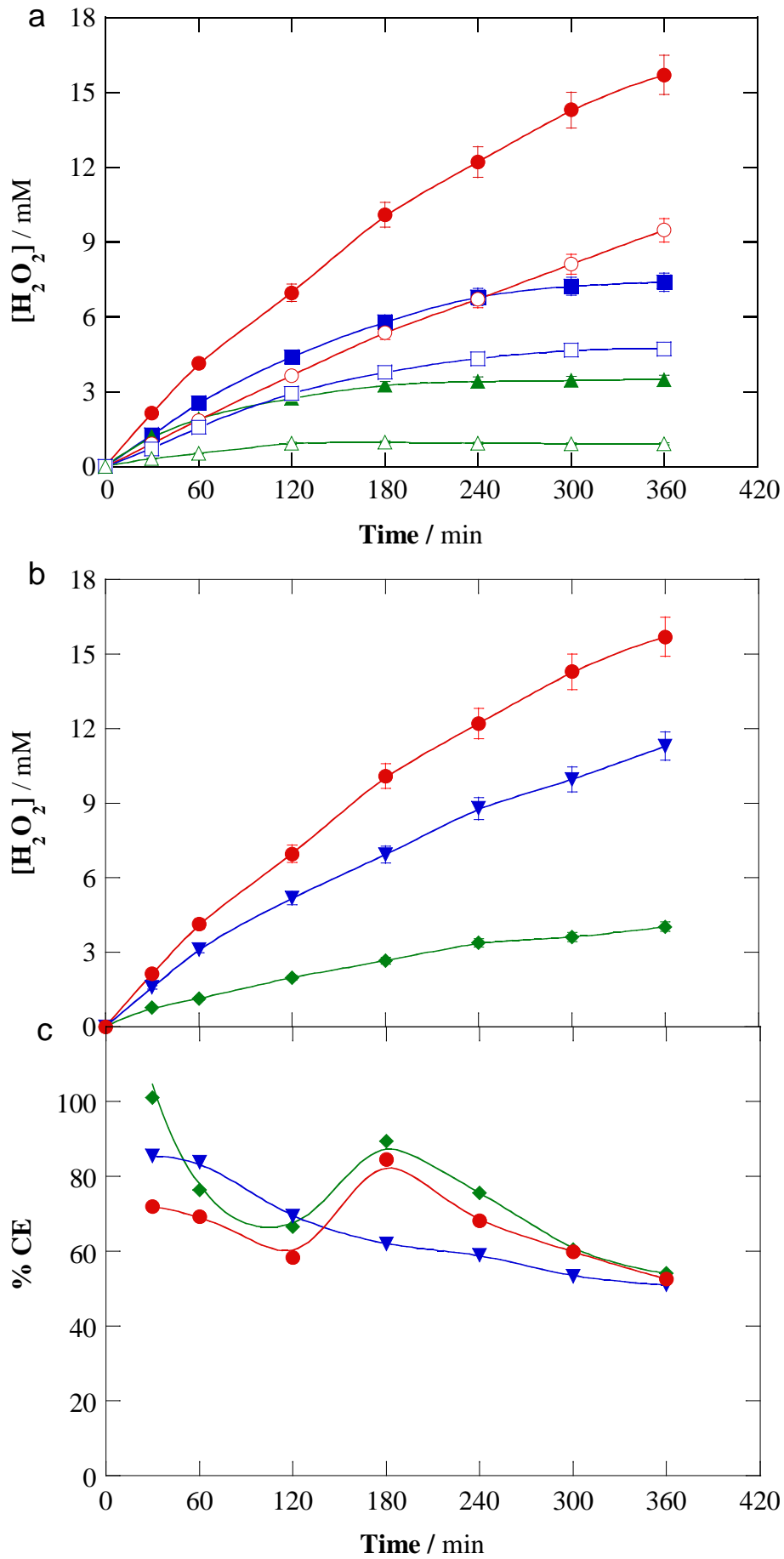
549   and liquid flow rate of 180 L h^{-1}.

550

Fig. 1

578
579
580
581
582
583
584
585
586
587
588
589
590
591
592
593
594
595
596
597
598
599
600
601
602 **Fig. 2**
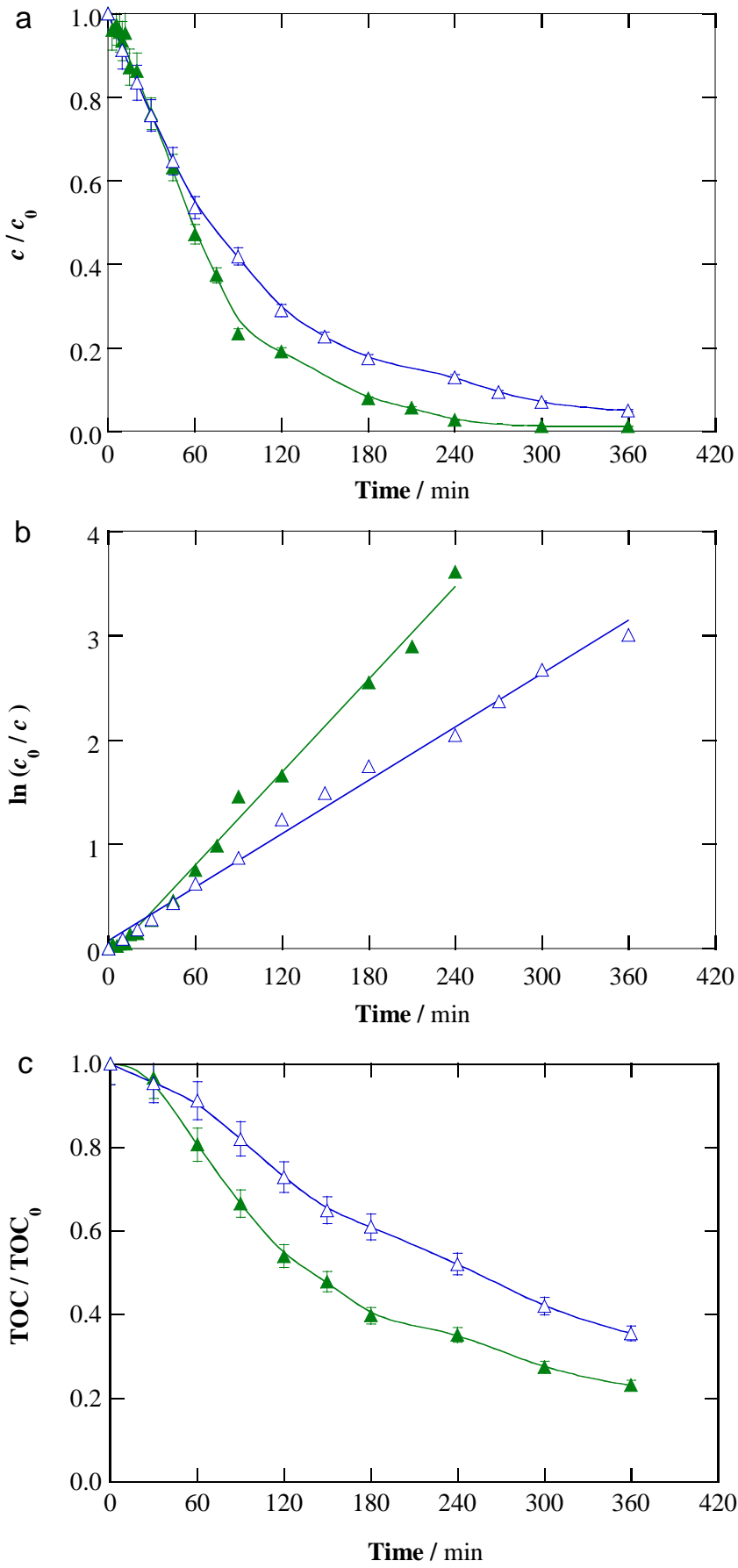
Fig. 3

628

629
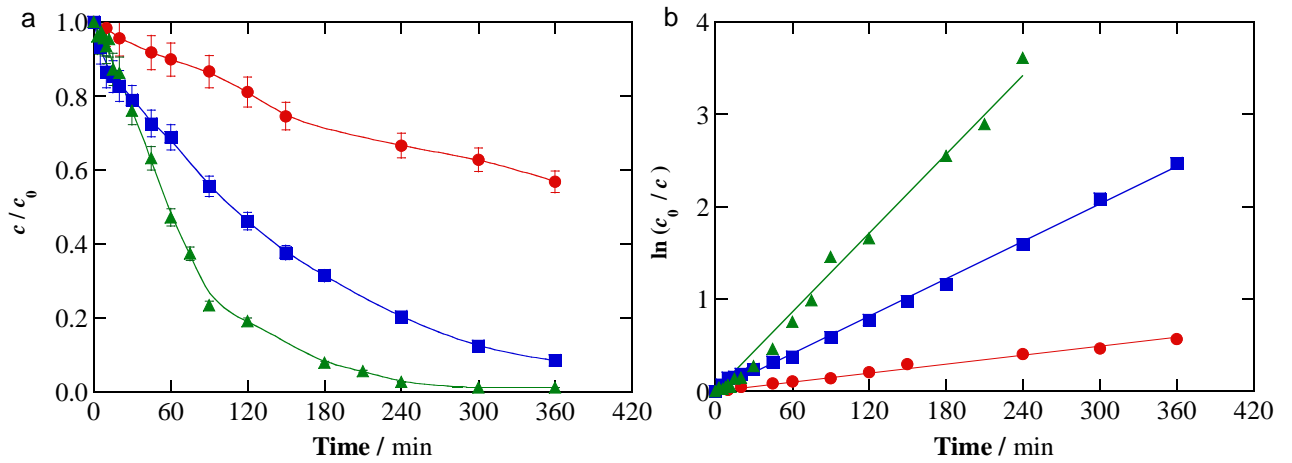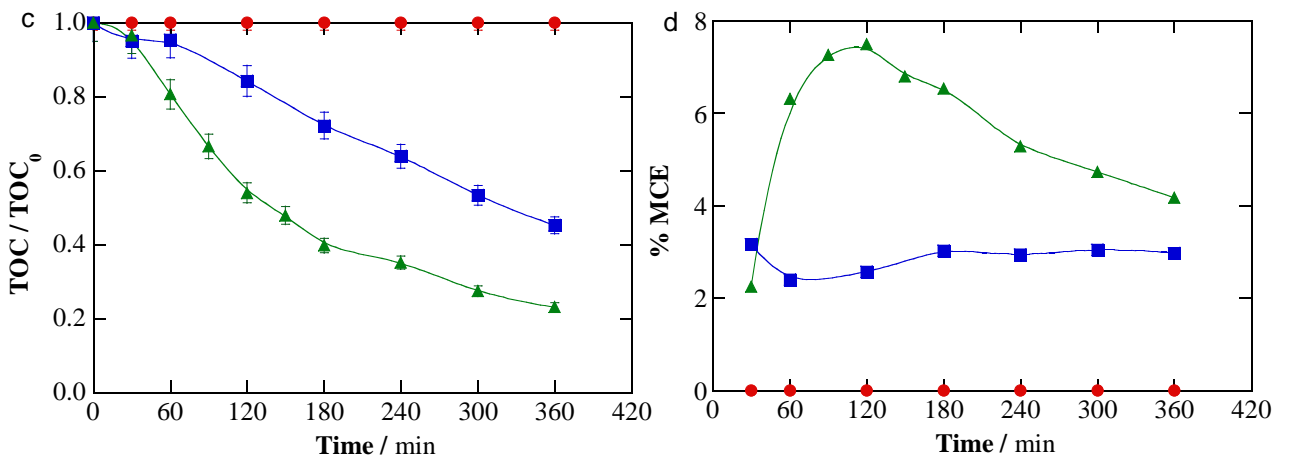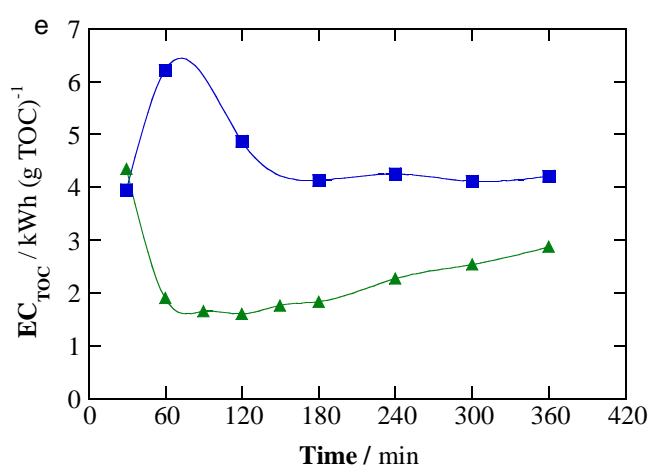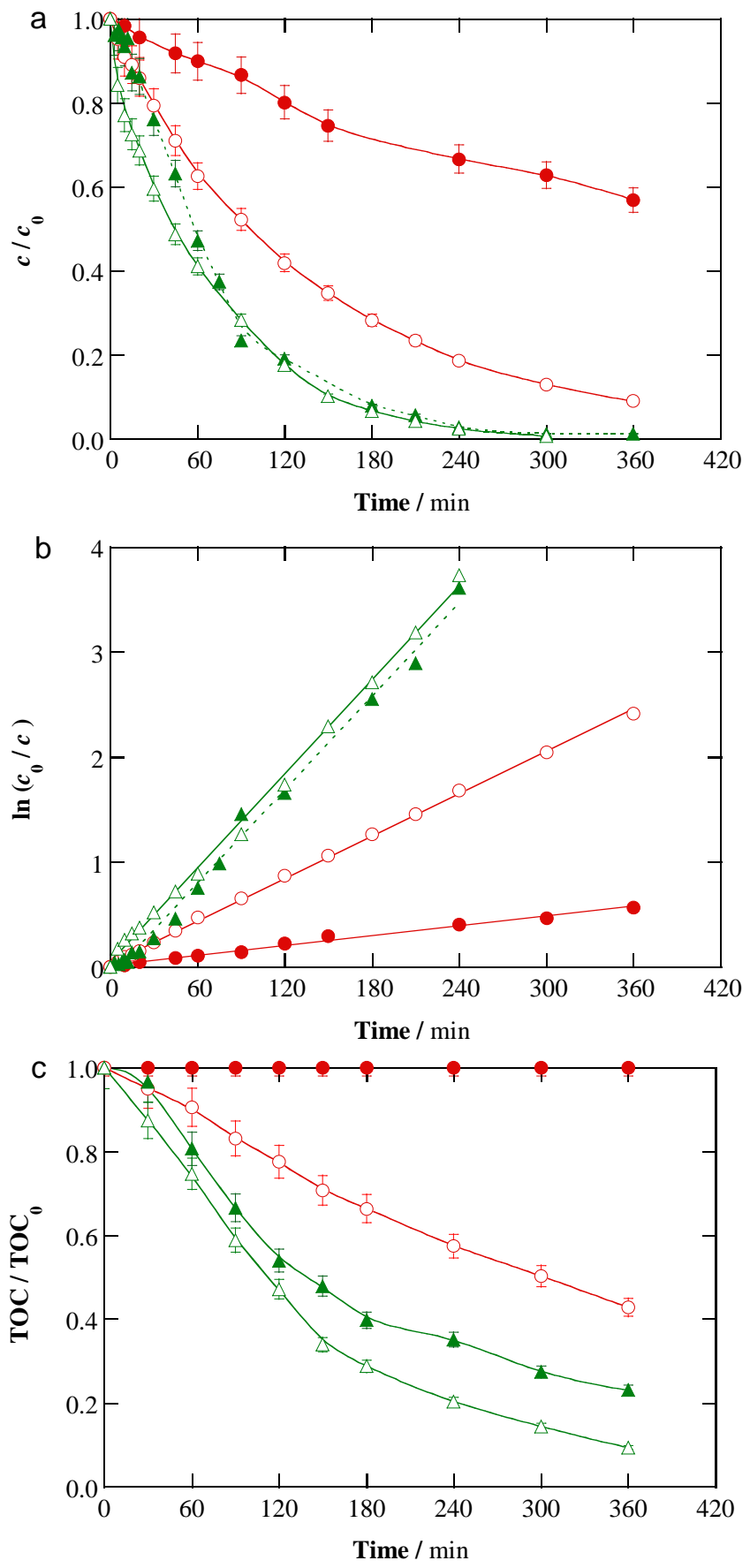
630

631

632

633

634

635

636

637

638

639

640

641

642

643

644

645

646

647

648

649

650

651

652

653

654 **Fig. 4**

655

656

657

658

659

660

661

662

663

664

665

666

667

668

669
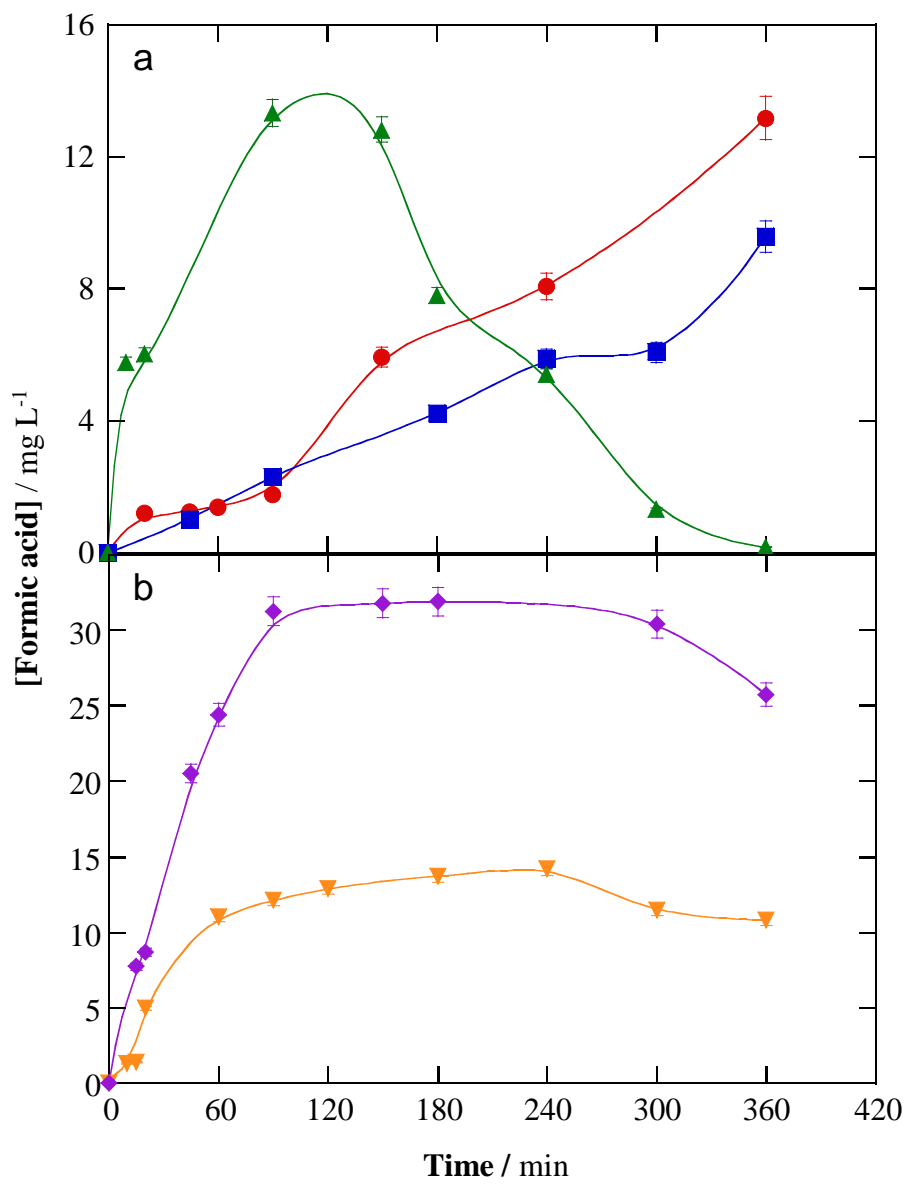
670

671

672

673

674

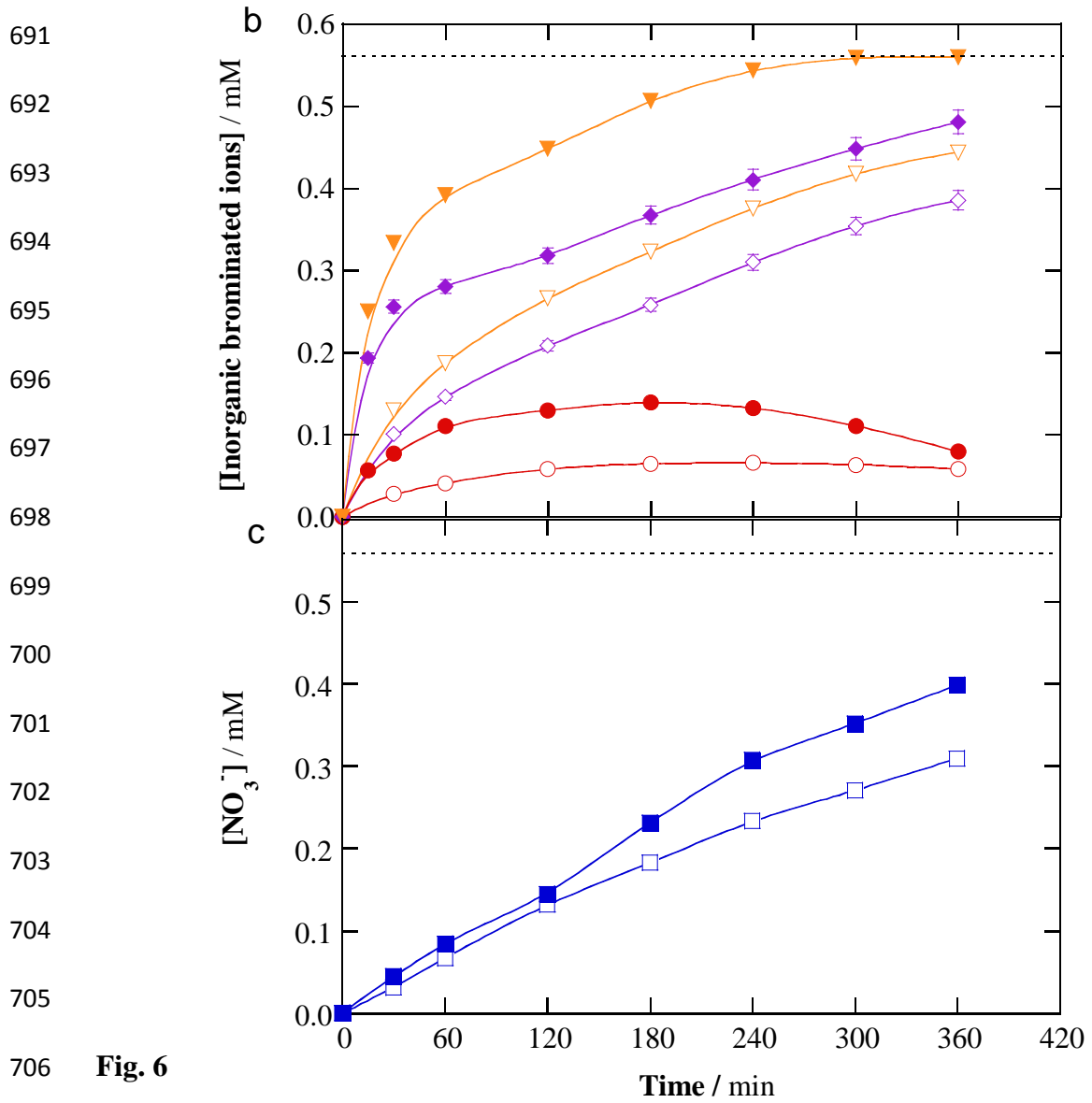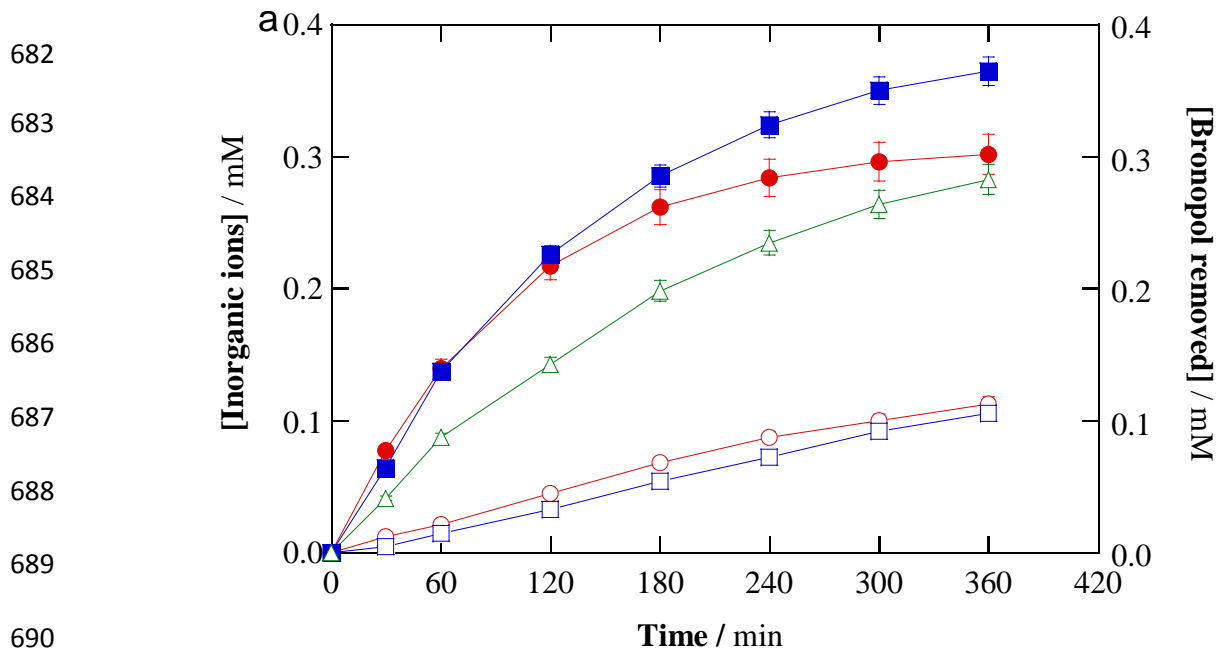675

676

677

678

679

680

681 **Fig. 5**

682
683
684
685
686
687
688
689
690
691
692
693
694
695
696
697
698
699
700
701
702
703
704
705
706

Fig. 6

707

708

709

716
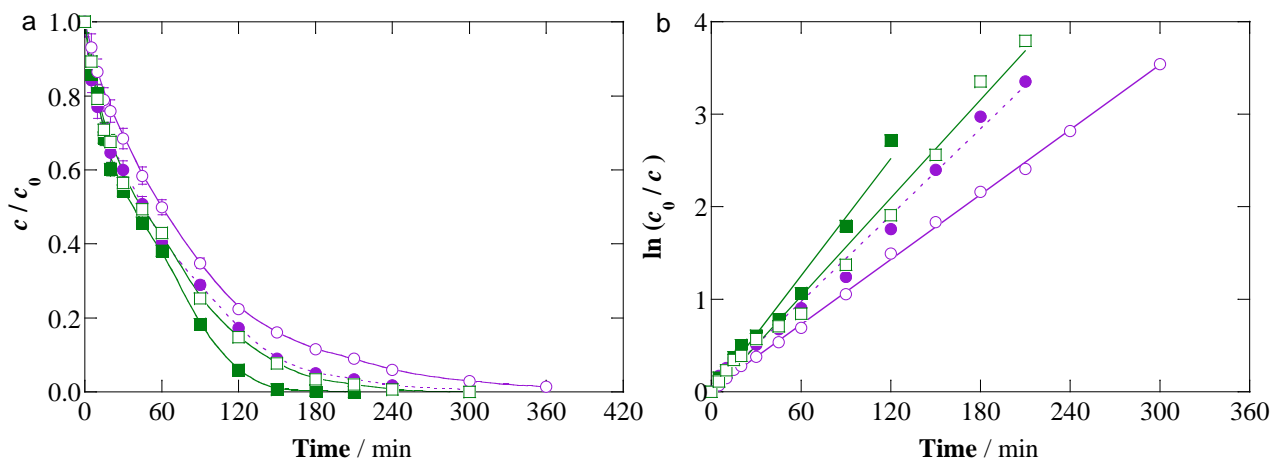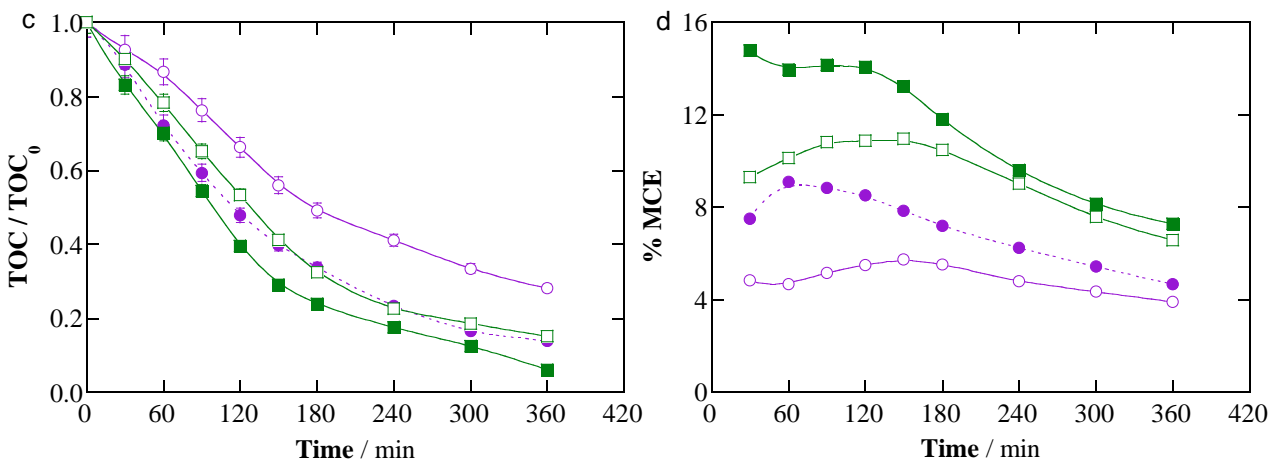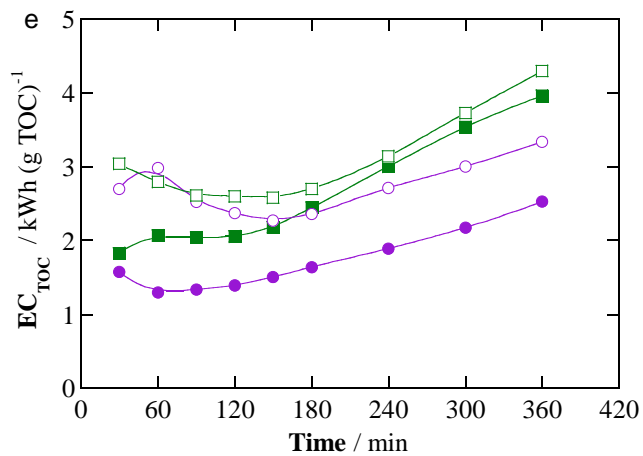
723

724

725

726

727

728

729

730

731

732

733 **Fig. 7**